Electronic Supplementary Material (ESI) for Environmental Science: Atmospheres.

Supporting Information: Dilution and Photooxidation Driven Processes Explain the Evolution of Organic Aerosol in Wildfire Plumes

Ali Akherati[1^], Yicong He[1], Lauren A. Garofalo[2], Anna L. Hodshire[2], Delphine K. Farmer[2], Sonia M. Kreidenweis[3], Wade Permar[4], Lu Hu[4], Emily V. Fischer[3], Coty N. Jen[5], Allen H. Goldstein[6], Ezra J. T. Levin[3], Paul J DeMott[3], Teresa L. Campos[7], Frank Flocke[7], John M. Reeves[7], Darin W. Toohey[8], Jeffrey R. Pierce[3*], and Shantanu H. Jathar[1*]

[1]Department of Mechanical Engineering, Colorado State University, Fort Collins, CO, USA
[2]Department of Chemistry, Colorado State University, Fort Collins, CO, USA
[3]Department of Atmospheric Science, Colorado State University, Fort Collins, CO, USA
[4]Department of Chemistry and Biochemistry, University of Montana, Missoula, MT, USA
[5]Department of Chemical Engineering, Carnegie Mellon University, Pittsburgh, PA, USA
[6]Department of of Environmental Science, Policy & Management, University of California Berkeley, Berkeley, CA, USA
[7]Earth Observing Laboratory, National Center for Atmospheric Research, Boulder, CO, USA
[8]Department of Atmospheric and Oceanic Science, University of Colorado Boulder, Boulder, CO, USA
[*]Correspondence to: Shantanu H. Jathar (shantanu.jathar@colostate.edu) and Jeffrey R. Pierce (jeffrey.pierce@colostate.edu)
[^]Now at the Department of Civil and Environmental Engineering, University of California Davis, Davis, CA, USA

Table S1: Precursor classes, surrogates, and parameters used in this work.

Precursor Class	***VOC Surrogate***	***ΔLVP***	m_{frag}	p_{1O}	p_{2O}	p_{3O}	p_{4O}	***Reference***
SVOCs	naphthalene	1.4922	0.7673	0.8138	0.0072	0.0635	0.1155	Zhang et al. (2014)
Linear alkanes	*n*-dodecane	1.4629	0.2627	0.9657	0.0010	0.0020	0.0314	Loza et al. (2014)
Benzene[&]	benzene	1.5495	0.7895	0.0743	0.0213	0.8963	0.0081	Ng et al. (2007)
Toluene[&]	toluene	1.4169	1.3064	0.5634	0.3413	0.0016	0.0937	Zhang et al. (2014)
C_{8+} single-ring aromatics[&]	*m*-xylene	1.4601	0.0736	0.1418	0.2971	0.4571	0.1040	Ng et al. (2007)
Multi-ring aromatics	naphthalene	1.4922	0.7673	0.8138	0.0072	0.0635	0.1155	Zhang et al. (2014)
Isoprene[^]	isoprene	1.8742	0.5207	0.9924	0.0003	0.0065	0.0009	Chhabra et al. (2011)
Terpene[^]	α-pinene	1.9139	0.1312	0.5991	0.2923	0.1079	0.0007	Chhabra et al. (2011)
Oxygenated aromatics	phenol, guaiacol	2.023	0.315	0.109	0.048	0.439	0.404	Yee et al.(2013)
Oxygenated aromatics	syringol	1.629	0.148	0.394	0.121	0.071	0.414	Yee et al. (2013)
Heterocyclics	2-methylfuran, dimethylfuran	1.459	0.449	0.0005	0.0014	0.998	0.0001	He et al. (2020)

[&]Together, aromatic hydrocarbons. [^]Together, biogenics.

Table S2: SOA precursors measured by the PTR-ToF-MS and included in the SOM-TOMAS model. Only the most dominant isomer is listed in the first column.

Species name	***Species formula***	k_{OH} ***[cm^3 molecules^{-1} s^{-1}]***	***MW [g mol^{-1}]***	***Surrogate***
Pyrrole	C_4H_5N	1.45×10^{-10}	67.09	Heterocyclics
Furan	C_4H_4O	4.00×10^{-11}	68.07	Heterocyclics
Isoprene	C_5H_8	1.00×10^{-10}	68.12	Biogenics
Dihydropyrrole	C_4H_7N	1.04×10^{-10}	69.10	Heterocyclics
Tetrahydropyrrole	C_4H_9N	7.85×10^{-11}	71.12	Heterocyclics
Benzene	C_6H_6	1.22×10^{-12}	78.11	Reduced Aromatics
Pyridine	C_5H_5N	3.70×10^{-13}	79.10	Heterocyclics
Methylpyrrole	C_5H_7N	1.10×10^{-10}	81.12	Heterocyclics
MethylFuran	C_5H_6O	7.80×10^{-11}	82.10	Heterocyclics
Furanone	$C_4H_4O_2$	5.66×10^{-11}	84.07	Heterocyclics
Toluene	C_7H_8	5.63×10^{-12}	92.14	Reduced Aromatics
2-Furancarbonitrile	C_5H_3NO	7.15×10^{-12}	93.08	Heterocyclics
MethylPyridine	C_6H_7N	1.10×10^{-12}	93.13	Heterocyclics
Phenol	C_6H_6O	2.80×10^{-11}	94.11	Oxygenated Aromatics
Furfural	$C_5H_4O_2$	3.55×10^{-11}	96.08	Heterocyclics
Dimethylfuran	C_6H_8O	2.00×10^{-10}	96.13	Heterocyclics
2-Methanolfuran	$C_5H_6O_2$	1.04×10^{-10}	98.10	Heterocyclics
Dihydrofurandione	$C_4H_4O_3$	8.56×10^{-13}	100.07	Heterocyclics
Benzonitrile	C_7H_5N	3.44×10^{-13}	103.12	Reduced Aromatics
Styrene	C_8H_8	5.80×10^{-11}	104.15	Reduced Aromatics
Vinylpyridine	C_7H_7N	2.66×10^{-11}	105.14	Heterocyclics
Benzaldehyde	C_7H_6O	1.20×10^{-11}	106.12	Oxygenated Aromatics
C8_Aromatics	C_8H_{10}	1.32×10^{-11}	106.16	Reduced Aromatics
Benzoquinone	$C_6H_4O_2$	4.51×10^{-12}	108.09	Oxygenated Aromatics
Cresol	C_7H_8O	5.30×10^{-11}	108.14	Oxygenated Aromatics
Benzenediol	$C_6H_6O_2$	1.04×10^{-10}	110.11	Oxygenated Aromatics
Trimethylfuran	$C_7H_{10}O$	1.59×10^{-10}	110.15	Heterocyclics
Dihydroxypyridine	$C_5H_5NO_2$	4.55×10^{-11}	111.10	Heterocyclics
5-Hydroxy 2-furfural	$C_5H_4O_3$	4.90×10^{-11}	112.08	Heterocyclics
Nitrofuran	$C_4H_3NO_3$	5.06×10^{-12}	113.07	Heterocyclics
5-Hydroxymethyl-2[3H]-furanone	$C_5H_6O_3$	1.00×10^{-10}	114.10	Heterocyclics
5-Hydroxytetrahydro2-furfural	$C_5H_8O_3$	5.00×10^{-12}	116.11	Heterocyclics
Benzeneacetonitrile	C_8H_7N	2.07×10^{-12}	117.15	Reduced Aromatics
Benzofuran	C_8H_6O	3.70×10^{-11}	118.13	Heterocyclics
Methylstyrene	C_9H_{10}	5.40×10^{-11}	118.18	Reduced Aromatics
Tolualdehyde	C_8H_8O	1.60×10^{-11}	120.15	Oxygenated Aromatics
C9 Aromatics	C_9H_{12}	2.20×10^{-11}	120.19	Reduced Aromatics
Salicylaldehyde	$C_7H_6O_2$	2.80×10^{-11}	122.12	Oxygenated Aromatics
Dimethylphenol	$C_8H_{10}O$	5.05×10^{-11}	122.16	Oxygenated Aromatics
Hydroxy benzoquinone	$C_6H_4O_3$	1.30×10^{-11}	124.09	Oxygenated Aromatics
Guaiacol	$C_7H_8O_2$	7.53×10^{-11}	124.14	Oxygenated Aromatics
Hydroxymethylfurfural	$C_6H_6O_3$	1.00×10^{-10}	126.11	Heterocyclics
Methyl benzofuran	C_9H_8O	9.75×10^{-11}	132.16	Heterocyclics
Methyl propenyl benzene	$C_{10}H_{12}$	3.30×10^{-11}	132.20	Reduced Aromatics
3-Methylacetophenone	$C_9H_{10}O$	2.42×10^{-12}	134.17	Oxygenated Aromatics

C10_Aromatics	$C_{10}H_{14}$	9.50×10^{-12}	134.22	Reduced Aromatics
Methylbenzoic Acid	$C_8H_8O_2$	1.20×10^{-11}	136.15	Oxygenated Aromatics
Monoterpenes	$C_{10}H_{16}$	1.63×10^{-10}	136.23	Biogenics
Nitrotoluene	$C_7H_7NO_2$	7.72×10^{-13}	137.13	Reduced Aromatics
Methylguaiacol	$C_8H_{10}O_2$	3.97×10^{-11}	138.16	Oxygenated Aromatics
Methylnaphthalene	$C_{11}H_{10}$	5.65×10^{-11}	142.20	Reduced Aromatics
Product of levoglucosan dehydration (pyrolysis)	$C_6H_8O_4$	5.28×10^{-11}	144.12	Alkanes
Dimethylbenzofuran	$C_{10}H_{10}O$	1.20×10^{-10}	146.18	Heterocyclics
Methylchavicol	$C_{10}H_{12}O$	5.43×10^{-11}	148.20	Oxygenated Aromatics
C11_aromatics	$C_{11}H_{16}$	5.00×10^{-11}	148.24	Reduced Aromatics
Vinylguaiacol	$C_9H_{10}O_2$	5.44×10^{-11}	150.17	Oxygenated Aromatics
Vanillin	$C_8H_8O_3$	2.73×10^{-11}	152.15	Oxygenated Aromatics
Camphor	$C_{10}H_{16}O$	4.30×10^{-12}	152.23	Biogenics
Syringol	$C_8H_{10}O_3$	9.66×10^{-11}	154.16	Oxygenated Aromatics
Cineole	$C_{10}H_{18}O$	2.26×10^{-11}	154.25	Biogenics
1,3-Dimethylnaphthalene	$C_{12}H_{12}$	6.94×10^{-11}	156.22	Reduced Aromatics
Decanal	$C_{10}H_{20}O$	3.45×10^{-11}	156.26	Alkanes
C12_aromatics	$C_{12}H_{18}$	1.13×10^{-10}	162.27	Reduced Aromatics
Isoeugenol	$C_{10}H_{12}O_2$	8.84×10^{-11}	188.22	Oxygenated Aromatics
C13_aromatics	$C_{13}H_{20}$	1.13×10^{-10}	176.30	Reduced Aromatics
Sesquiterpenes	$C_{15}H_{24}$	3.00×10^{-10}	204.35	Biogenics
5-MethylFurfural	$C_6H_6O_2$	5.18×10^{-11}	110.11	Heterocyclics

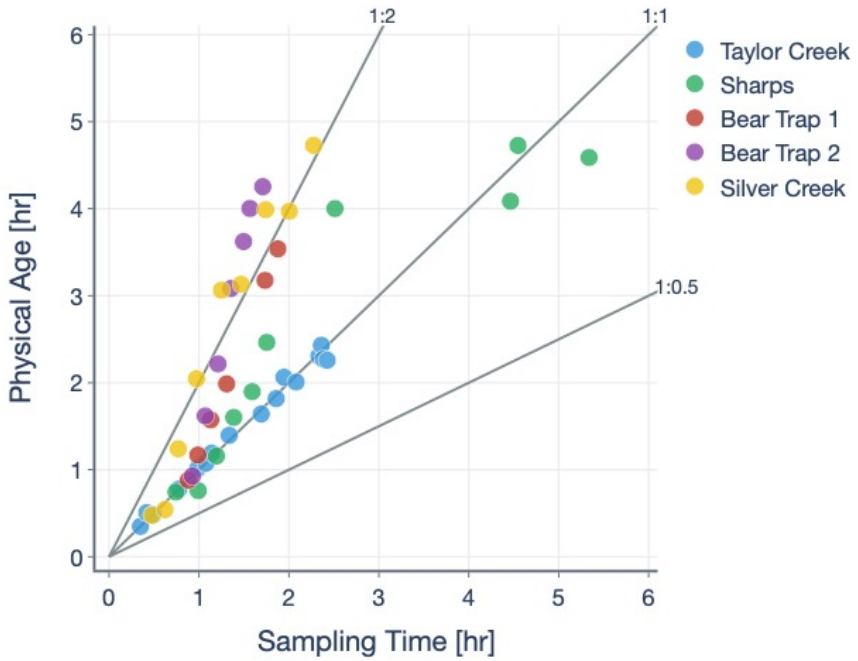

Figure S1: Physical age plotted against the sampling time for the five transect sets and four wildfire plumes. Physical age was calculated by dividing the straight-line distance from the fire with the average wind speed measured within a transect. Sampling time was calculated as the time of the day minus the time when the first transect was sampled but offset by the physical age at the first transect.

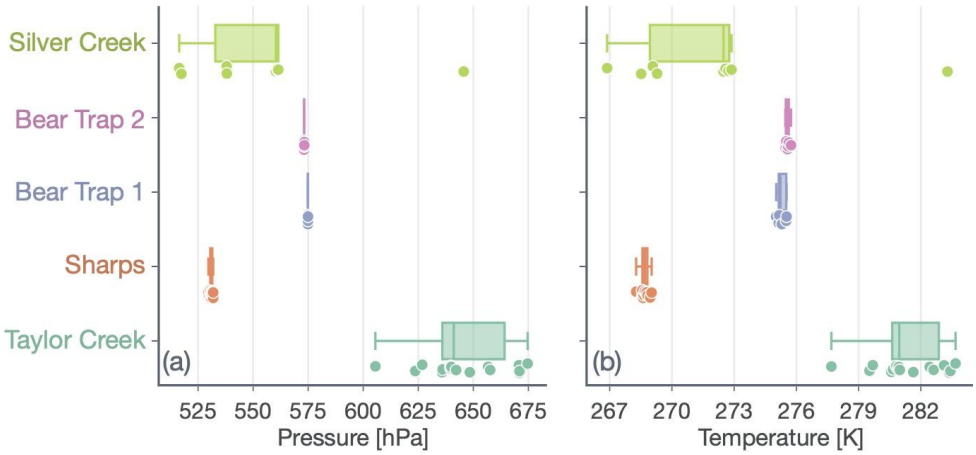

Wildfire	*Average Pressure [hPa]*	*Average Temperature [K]*
Taylor Creek	646	281.4
Sharps	531	268.7
Bear Trap 1	575	275.3
Bear Trap2	573	275.6
Silver Creek	555	272.0

Figure S2: Box plots for (a) pressures and (b) temperatures encountered during the pseudo-Lagrangian evolution of smoke in the five transect sets and four wildfire plumes.

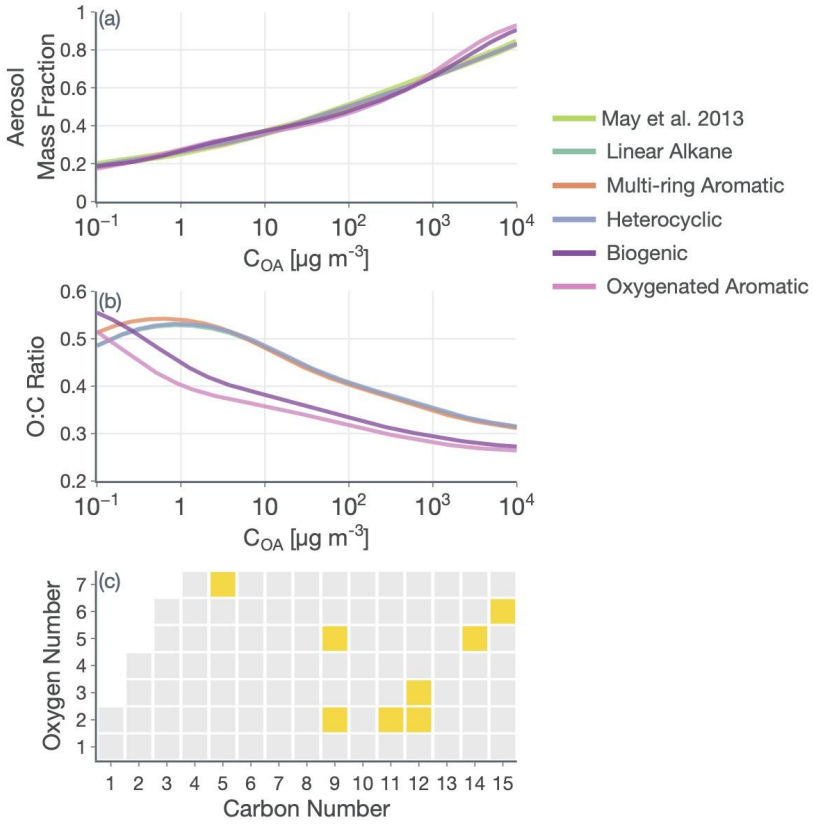

Figure S3: (a) POA volatility from May et al. (2013) and that used in this work expressed as the aerosol mass fraction against the OA mass concentration. The POA volatility based on the use of multi-ring aromatics was used with the base configuration of the SOM-TOMAS model while the POA volatility based on the use of other organic classes was used to perform sensitivity simulations. (b) Dependence of the OA O:C ratio as a function of the OA mass concentration. (c) Model species, shown in yellow, in the SOM grid used to represent the POA and SVOC mass. This distribution was informed based on the Monte-Carlo simulations performed and discussed in Section 3.2 in the main paper.

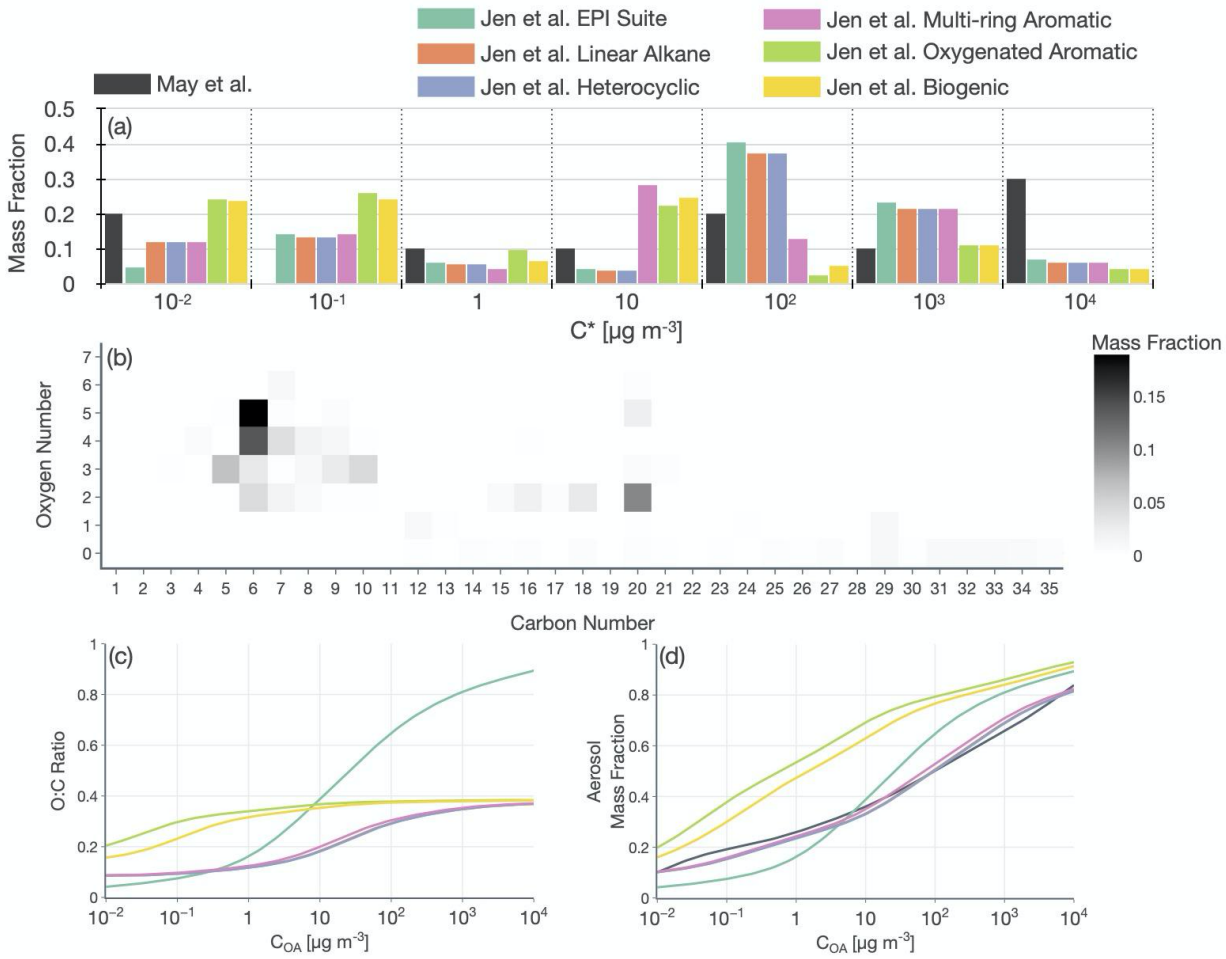

Figure S4: Averaged and normalized, (a) volatility distribution and (b) mass distribution in carbon-oxygen space for the POA and SVOC emissions quantified by Jen et al. (2019). Volatility distribution from May et al. (2014) is also presented in panel (a). POA (c) O:C ratio and (d) aerosol mass fraction as a function of the OA mass concentration. Jen et al. (2019) only quantified 10 to 65% of the POA and SVOC mass collected on quartz filters. The volatility (c^*) was calculated for the POA and SVOC species either using EPISuite v4.11 (EPA, 2021) or the Statistical Oxidation Model (SOM) (Cappa and Wilson, 2012; Jathar et al., 2015).

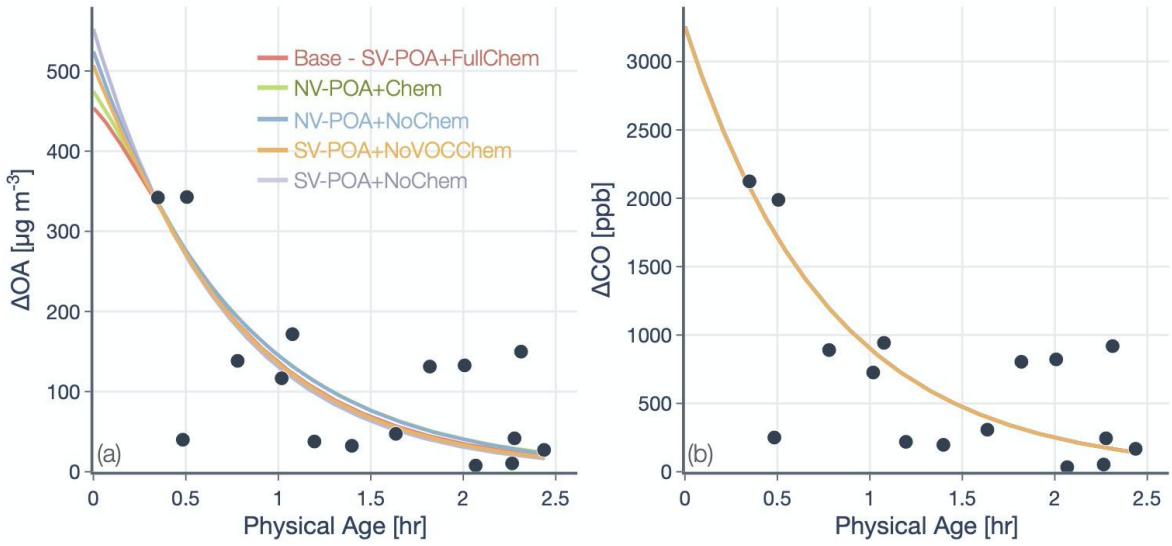

Figure S5: Predictions of the (a) OA and (b) CO concentrations from the SOM-TOMAS model (solid-colored lines) compared against measurements (solid black circles) from the Taylor Creek Fire. Model predictions are shown for five different simulations that vary in their assumptions about POA volatility and oxidation chemistry.

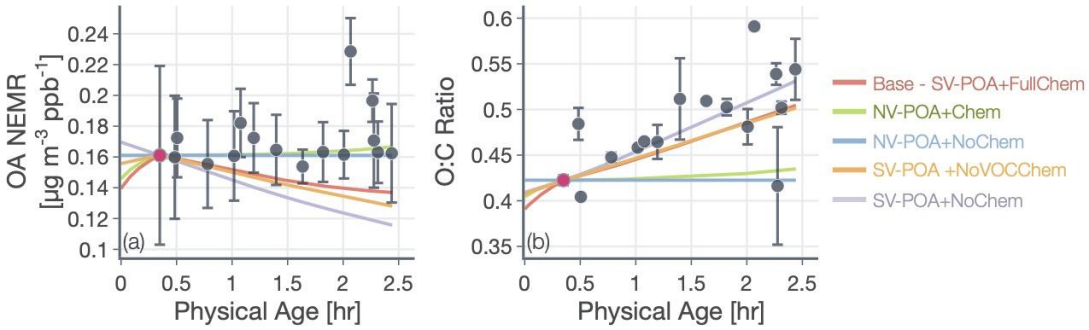

Figure S6: Same as Figure 4 but with the standard error in the mean for the observations.

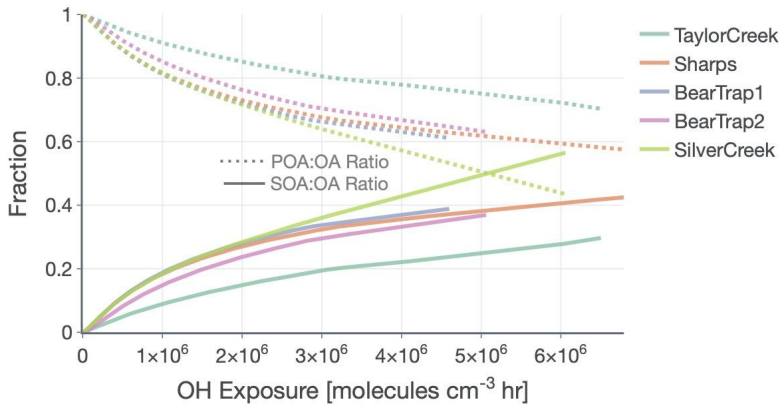

Figure S7: Predicted POA (dotted lines) and SOA (solid lines) ratios with OA for the base simulation results presented in Figures 4 and 5.

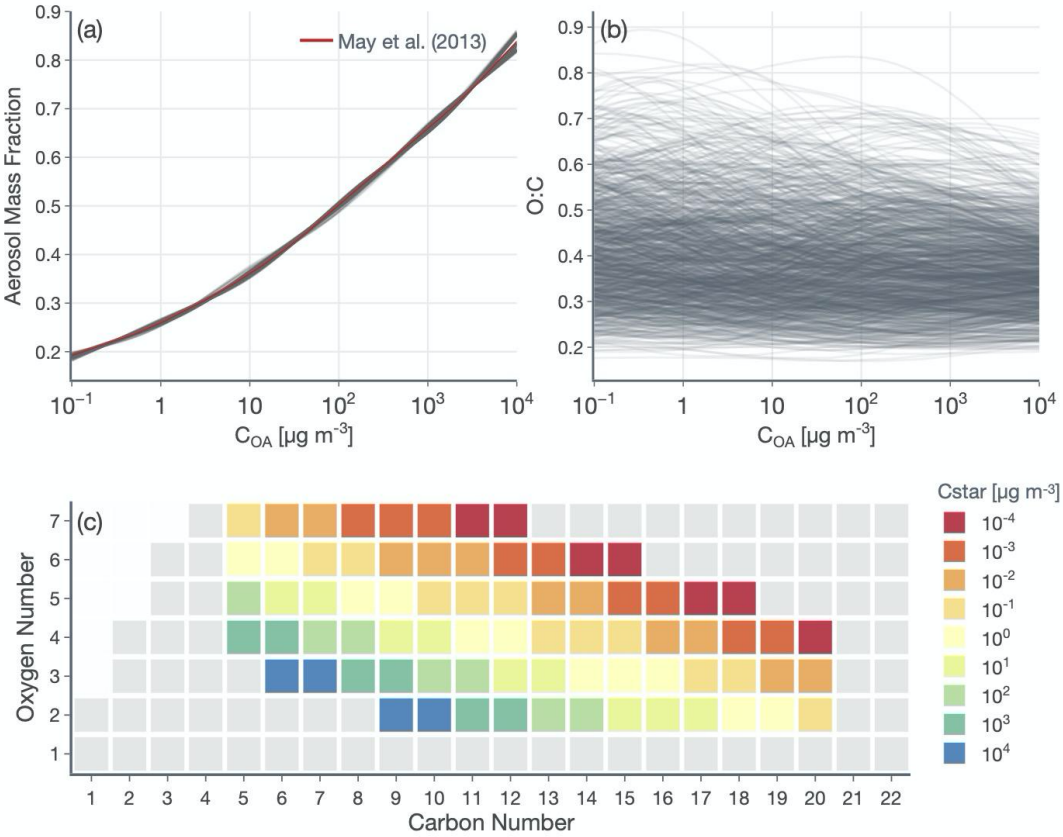

Figure S8: (a) POA volatility from May et al. (2013) and that based on 1000 Monte Carlo simulations. (b) OA O:C ratio as a function of the OA mass concentration for all 1000 Monte Carlo simulations. (c) SOM model species, shown in color, considered as options to represent the POA+SVOC mass.

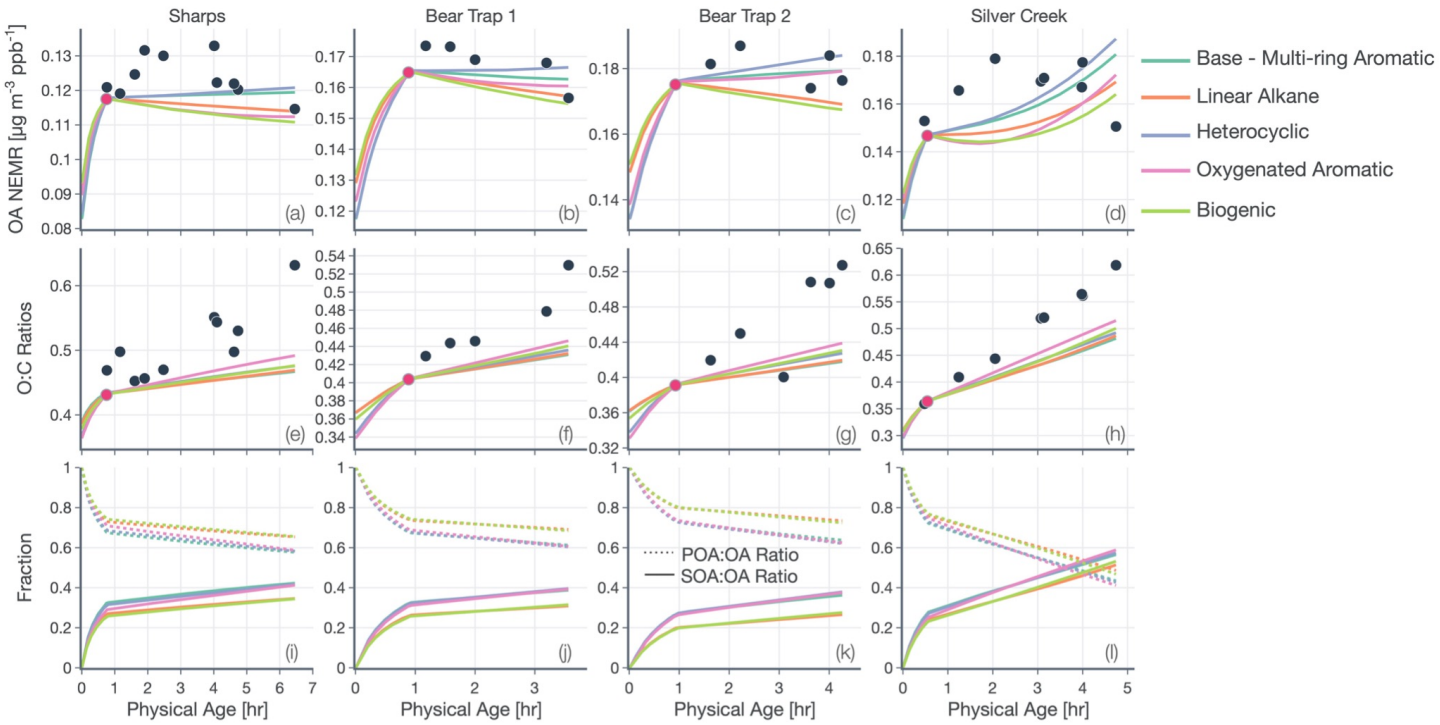

Figure S9: Predictions of (a,b,c,d) OA NEMR and (e,f,g,h) OA O:C from the SOM-TOMAS model (solid colored lines) compared against measurements (solid black circles) from the four different transect sets. (i,j,k,l) Predictions of the fractional contributions of POA and SOA to OA. Model predictions are shown for sensitivity simulations performed with varying assumptions for the SVOC oxidation chemistry.

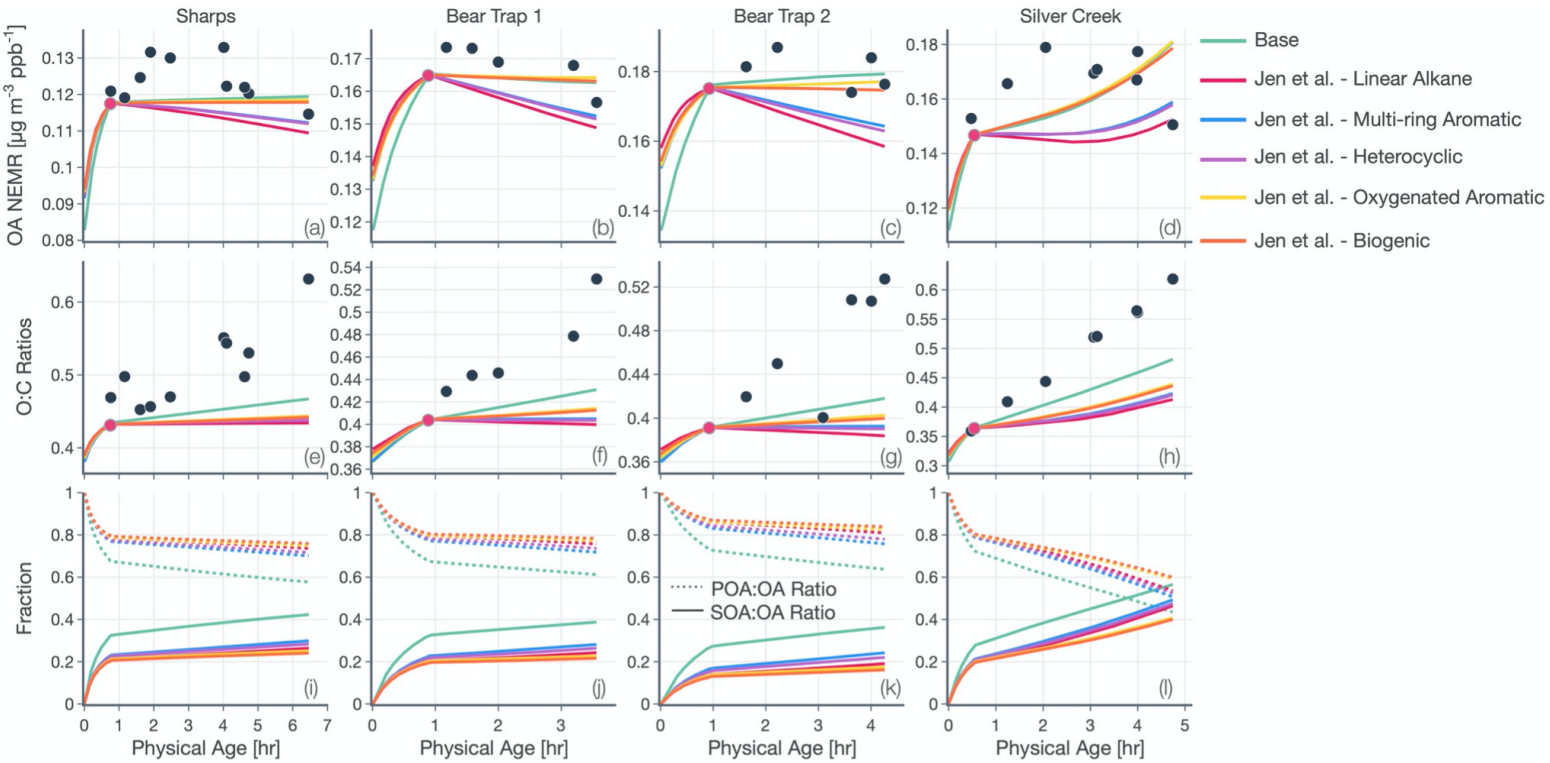

Figure S10: Predictions of (a,b,c,d) OA NEMR and (e,f,g,h) OA O:C from the SOM-TOMAS model (solid colored lines) compared against measurements (solid black circles) from the four different transect sets. (i,j,k,l) Predictions of the fractional contributions of POA and SOA to OA. Model predictions are shown for sensitivity simulations performed with varying assumptions for the POA volatility and SVOC oxidation chemistry.

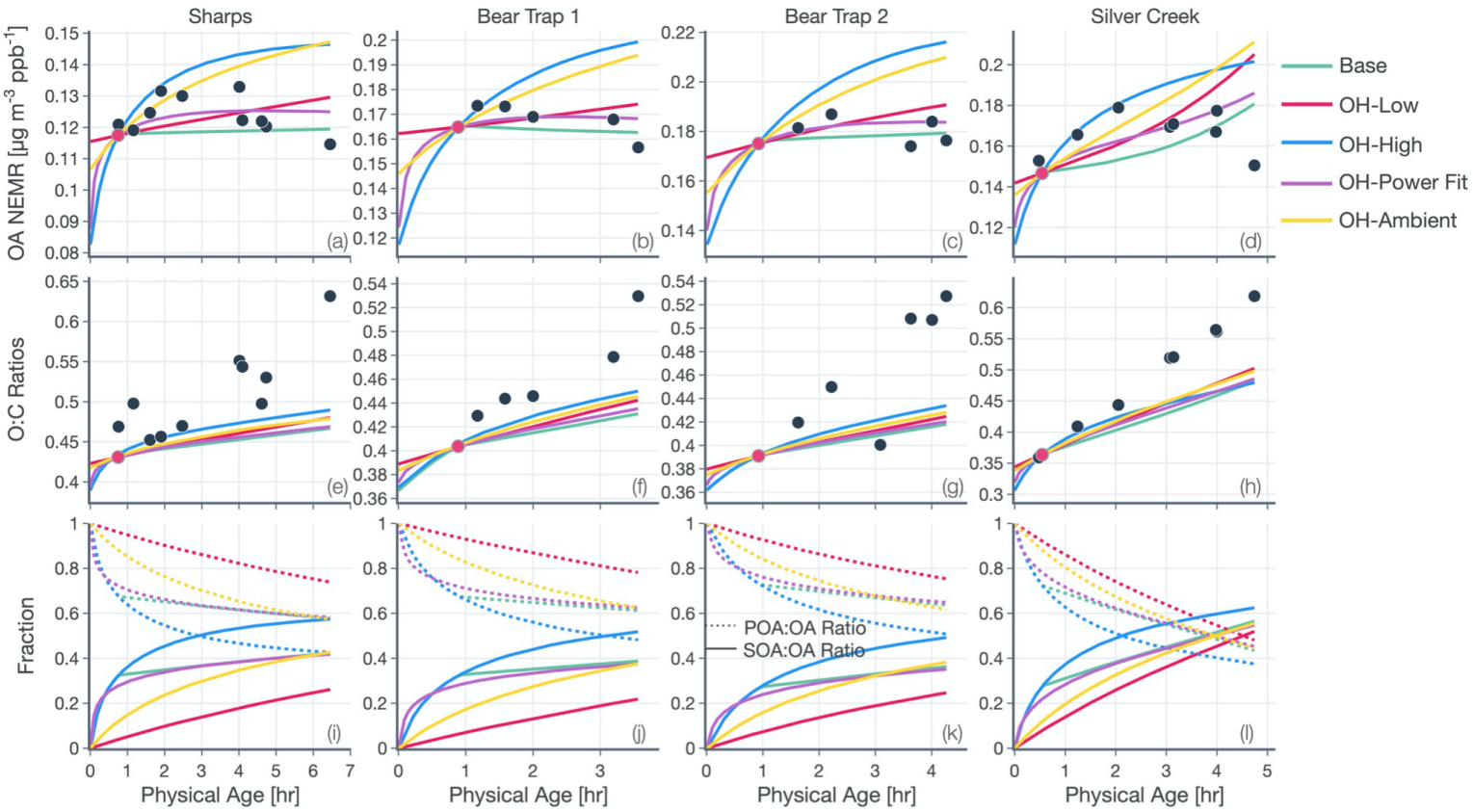

Figure S11: Predictions of (a,b,c,d) OA NEMR and (e,f,g,h) OA O:C from the SOM-TOMAS model (solid colored lines) compared against measurements (solid black circles) from the four different transect sets. (i,j,k,l) Predictions of the fractional contributions of POA and SOA to OA. Model predictions are shown for sensitivity simulations performed with varying assumptions for OH.

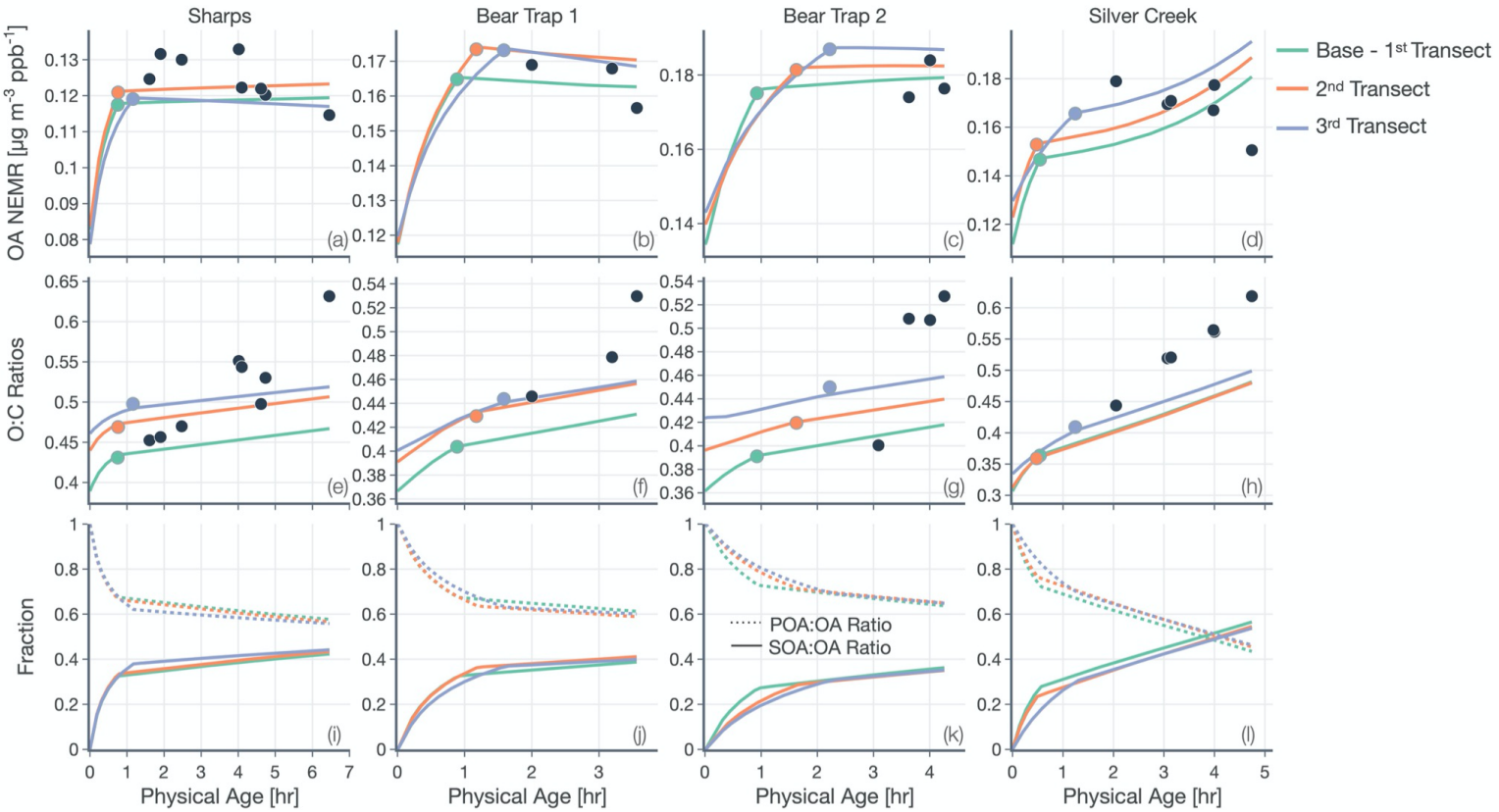

Figure S12: Predictions of (a,b,c,d) OA NEMR and (e,f,g,h) OA O:C from the SOM-TOMAS model (solid colored lines) compared against measurements (solid black circles) from the four different transect sets. (i,j,k,l) Predictions of the fractional contributions of POA and SOA to OA. Model predictions are shown for sensitivity simulations performed by varying the 'first transect'.

References

Cappa, C. D. and Wilson, K. R.: Multi-generation gas-phase oxidation, equilibrium partitioning, and the formation and evolution of secondary organic aerosol, Atmos. Chem. Phys., 12(20), 9505–9528, doi:10.5194/acp-12-9505-2012, 2012.

Chhabra, P. S., Ng, N. L., Canagaratna, M. R., Corrigan, A. L., Russell, L. M., Worsnop, D. R., Flagan, R. C. and Seinfeld, J. H.: Elemental composition and oxidation of chamber organic aerosol, Atmos. Chem. Phys., 11(17), 8827–8845, doi:10.5194/acp-11-8827-2011, 2011.

EPA: EPI Suite^{TM}-estimation program interface, [online] Available from: https://www.epa.gov/tsca-screening-tools/epi-suitetm-estimation-program-interface (Accessed 20 March 2021), 2021.

He, Y., King, B., Pothier, M., Lewane, L., Akherati, A., Mattila, J., Farmer, D. K., McCormick, R. L., Thornton, M., Pierce, J. R., Volckens, J. and Jathar, S. H.: Secondary organic aerosol formation from evaporated biofuels: comparison to gasoline and correction for vapor wall losses, Environ. Sci. Process. Impacts, In press, doi:10.1039/d0em00103a, 2020.

Jathar, S. H., Cappa, C. D., Wexler, A. S., Seinfeld, J. H. and Kleeman, M. J.: Multi-generational oxidation model to simulate secondary organic aerosol in a 3-D air quality model, Geoscientific Model Development; Katlenburg-Lindau, 8(8), 2553–2567, doi:10.5194/gmd-8-2553-2015, 2015.

Jen, C. N., Hatch, L. E., Selimovic, V., Yokelson, R. J., Weber, R., Fernandez, A. E., Kreisberg, N. M., Barsanti, K. C. and Goldstein, A. H.: Speciated and total emission factors of particulate organics from burning western US wildland fuels and their dependence on combustion efficiency, Atmos. Chem. Phys., 19(2), 1013–1026, doi:10.5194/acp-19-1013-2019, 2019.

Loza, C. L., Craven, J. S., Yee, L. D., Coggon, M. M., Schwantes, R. H., Shiraiwa, M., Zhang, X., Schilling, K. A., Ng, N. L., Canagaratna, M. R., Ziemann, P. J., Flagan, R. C. and Seinfeld, J. H.: Secondary organic aerosol yields of 12-carbon alkanes, Atmos. Chem. Phys., 14(3), 1423–1439, doi:10.5194/acp-14-1423-2014, 2014.

May, A. A., Levin, E. J. T., Hennigan, C. J., Riipinen, I., Lee, T., Collett, J. L., Jimenez, J. L., Kreidenweis, S. M. and Robinson, A. L.: Gas-particle partitioning of primary organic aerosol emissions: 3. Biomass burning, J. Geophys. Res. D: Atmos., 118(19) [online] Available from: http://onlinelibrary.wiley.com/doi/10.1002/jgrd.50828/full, 2013.

Ng, N. L., Kroll, J. H., Chan, A. W. H., Chhabra, P. S., Flagan, R. C. and Seinfeld, J. H.: Secondary organic aerosol formation from m-xylene, toluene, and benzene, Atmos. Chem. Phys., 7(14), 3909–3922, doi:10.5194/acp-7-3909-2007, 2007.

Yee, L. D., Kautzman, K. E., Loza, C. L., Schilling, K. A., Coggon, M. M., Chhabra, P. S., Chan, M. N., Chan, A. W. H., Hersey, S. P., Crounse, J. D., Wennberg, P. O., Flagan, R. C. and Seinfeld, J. H.: Secondary organic aerosol formation from biomass burning intermediates: phenol and methoxyphenols, Atmos. Chem. Phys., 13(16), 8019–8043, doi:10.5194/acp-13-8019-2013, 2013.

Zhang, X., Cappa, C. D., Jathar, S. H., McVay, R. C., Ensberg, J. J., Kleeman, M. J. and Seinfeld, J. H.: Influence of vapor wall loss in laboratory chambers on yields of secondary organic aerosol, Proc. Natl. Acad. Sci. U. S. A., 111(16), 5802–5807, doi:10.1073/pnas.1404727111, 2014.